Bonding Hierarchy and Coordination Interaction Leading to High Thermoelectricity in Wide Band Gap $TlAgI_2$

Xiaoying Wang,[1] Mengyang Li,[2] Wen Shi,[3,4] Minxuan Feng,[1] Xuejie Li,[1] Yuzhou Hao,[1] Jiangang He,[5] Jun Sun,[1] Xiangdong Ding,[1] and Zhibin Gao[1, †]

[1]State Key Laboratory for Mechanical Behavior of Materials, School of Materials Science and Engineering, Xi'an Jiaotong University, Xi'an 710049, China

[2]School of Physics, Xidian University, Xi'an710071, China

[3]School of Chemistry, Sun Yat-sen University, Guangzhou, Guangdong, 510006, China

[4]Institute of Green Chemistry and Molecular Engineering, Sun Yat-sen University, Guangzhou, Guangdong, 510006, China

[5]School of Mathematics and Physics, University of Science and Technology Beijing, Beijing 100083, China

[†] E-mail: zhibin.gao@xjtu.edu.cn

Calculation details of potential wall:

Potential energy wall versus slight perturbations to different atoms are made depending on the direction of their phonon vibration. If the structure is relaxed after imposing a slight perturbation, it would revert to its initial energy minimum state through structure relaxation. We perturb the structure, perturbing the structure every 0.01 Å until the deformation is 0.15 Å.

Table SI. The detailed statistics of lattice thermal conductivity were obtained utilizing distinct definitions for harmonic approximation and self-consistent theory, spanning the temperature range from 100 K to 1200 K.

Temperature (K)	**HA**	κ_p^{3ph}	κ_p^{3+4ph}	κ_c	$\kappa_p^{3+4ph}+\kappa_c$	$\kappa_c/\kappa_p^{3+4ph}$
100	0.610	0.647	0.550	0.055	0.657	0.100
200	0.298	0.385	0.312	0.062	0.374	0.199
300	0.198	0.301	0.233	0.066	0.299	0.284
400	0.148	0.261	0.192	0.069	0.262	0.361
500	0.119	0.237	0.167	0.072	0.238	0.429
600	0.099	0.221	0.150	0.073	0.224	0.487
700	0.085	0.211	0.136	0.075	0.210	0.550
800	0.074	0.203	0.123	0.076	0.199	0.616
900	0.066	0.197	0.119	0.077	0.197	0.647
1000	0.059	0.193	0.113	0.078	0.192	0.692
1100	0.054	0.188	0.108	0.079	0.188	0.734
1200	0.049	0.186	0.104	0.080	0.183	0.774

Table SII. Bader charge analysis of various atoms in wide band gap $TlAgI_2$. The original number of valence electrons for each atom is derived from the POTCAR file, as indicated in column 2. The formation of compounds involving different atoms results in a change in the number of valence electrons, as illustrated in column 3. The gain/loss of electrons by different atoms and their valence states in compounds are presented in columns 4 and 5.

Atom	Original valence electron number	Valence electron results of bader charge	Gain/loss electrons	Valence state
Tl	3	2.75	Loss 0.25	+0.25
Tl	3	2.75	Loss 0.25	+0.25
Ag	11	11.28	Gain 0.28	-0.28
Ag	11	11.28	Gain 0.28	-0.28
I	7	7.10	Gain 0.10	-0.10
I	7	6.87	Loss 0.13	+0.13
I	7	7.10	Gain 0.10	-0.10
I	7	6.87	Loss 0.13	+0.13

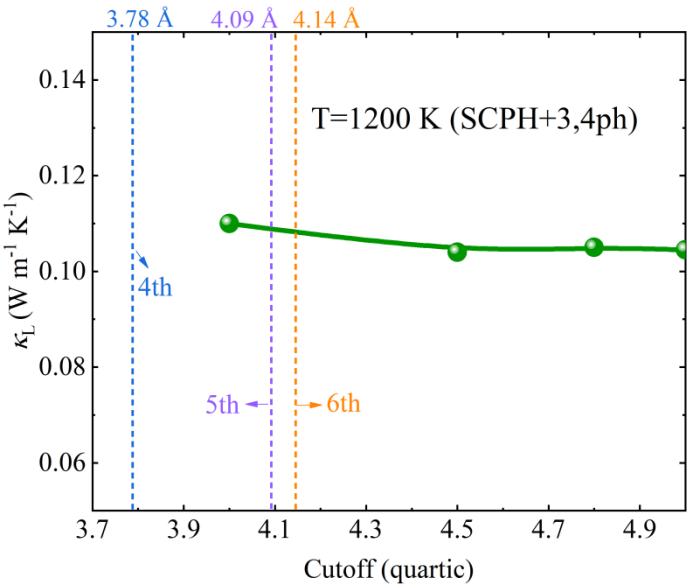

Figure. S1. The convergence test using different quartic cutoffs when calculating the lattice thermal conductivity with the self-consistent theory, considering third- and fourth-order phonon-phonon interactions (SCPH+3,4ph), the dashed line are actual cutoff.

To ensure the good convergence of quartic interatomic force constants (IFCs), we calculated the lattice thermal conductivity with different quartic cutoff distances, as shown in Figure. S1. The correct distances for the nearest-, second-nearest, and third-nearest neighbour are 2.82 Å (second), 3.54 Å (third) and 3.78 Å (fourth), respectively. Subsequently, the distances are 4.09 Å (fifth), 4.14 Å (sixth), 5.57 Å (seventh), 6.00 Å (eighth).

For our calculations of phonon thermal conductivity, we chose harmonic, cubic, and quartic cutoffs of 11.0 Å, 6.00 Å and 4.50 Å, respectively. The quartic cutoff of 4.50 Å that we selected is indeed larger than the actual quartic cutoff distance of 3.78 Å. The actual cutoff distances are indicated by the dashed line in Figure. S1.

In our previous manuscript, we selected a quartic phonon anharmonicity cutoff of 4.50 Å, which we considered sufficient for convergence. We chose a slightly larger cutoff distance than the actual one to account for more interatomic interactions, ensuring the force constants converge, regardless of whether atoms exist between the 4.5-5.0 Å shell. Therefore, our previous manuscript choice of 4.5 Å for the quartic phonon anharmonicity cutoff is deemed sufficient for convergence.

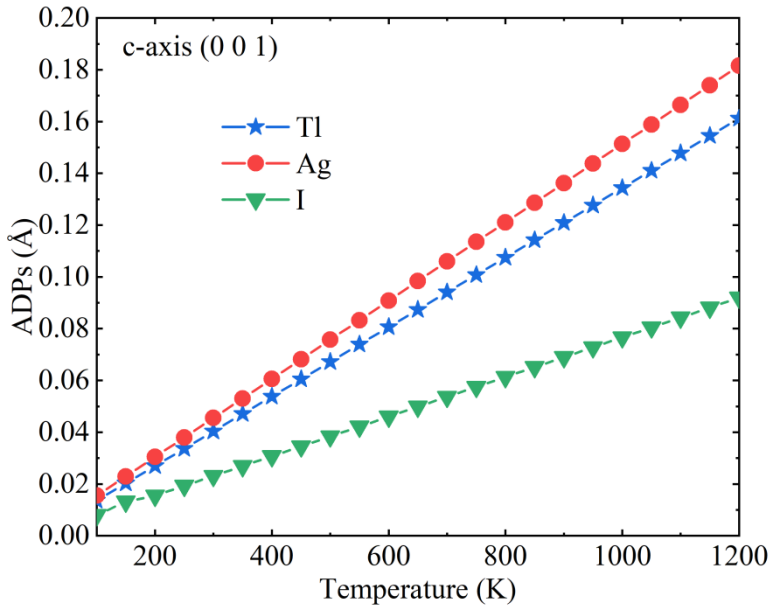

Figure. S2. Atomic displacement parameters (ADP) of different atoms along the *c*-axis direction. The colors blue, red, and green correspond to Tl, Ag, and I atoms, respectively.

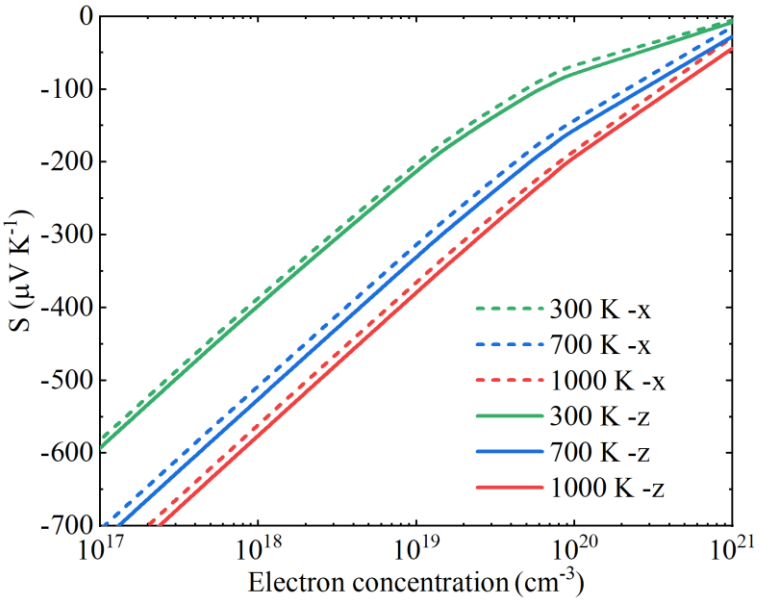

Figure. S3. The electronic transport performance of Seebeck coefficient for *n*-type $TlAgI_2$ along *x*- and *z*-direction at 300 K, 700 K, and 1000 K, respectively by HSE06 functional.

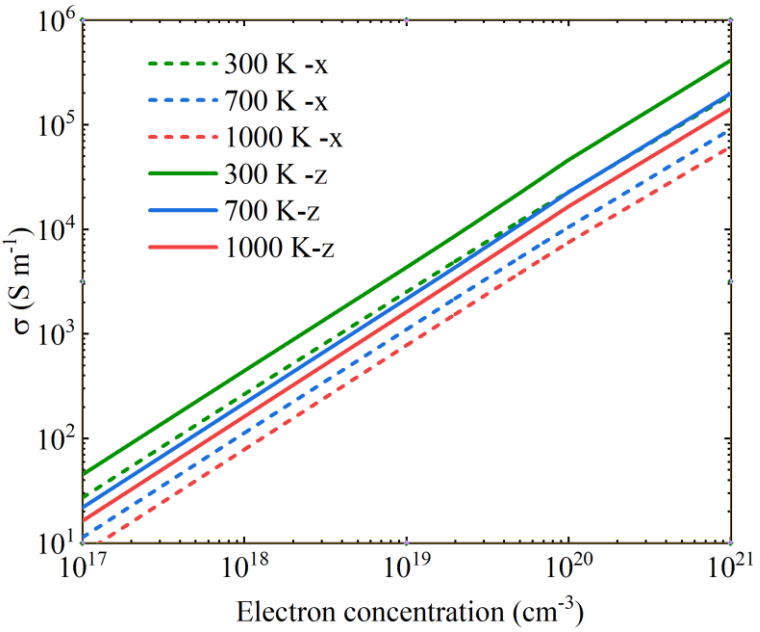

Figure. S4. The electronic transport performance of conductivity for *n*-type $TlAgI_2$ along *x*- and *z*-direction at 300 K, 700 K, and 1000 K, respectively by HSE06 functional.

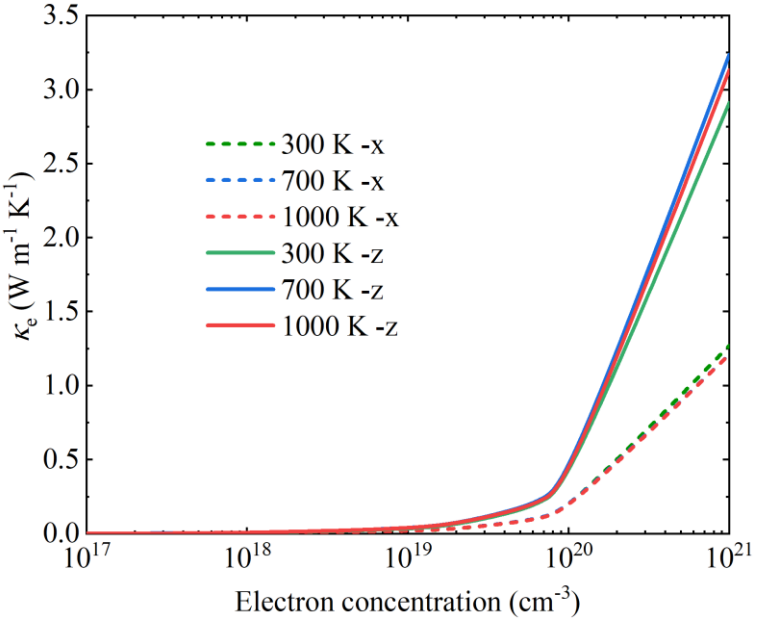

Figure. S5. The electronic transport performance of electronic thermal conductivity along *x*- and *z*-direction for *n*-type $TlAgI_2$ at 300 K, 700 K, and 1000 K, respectively by HSE06 functional.

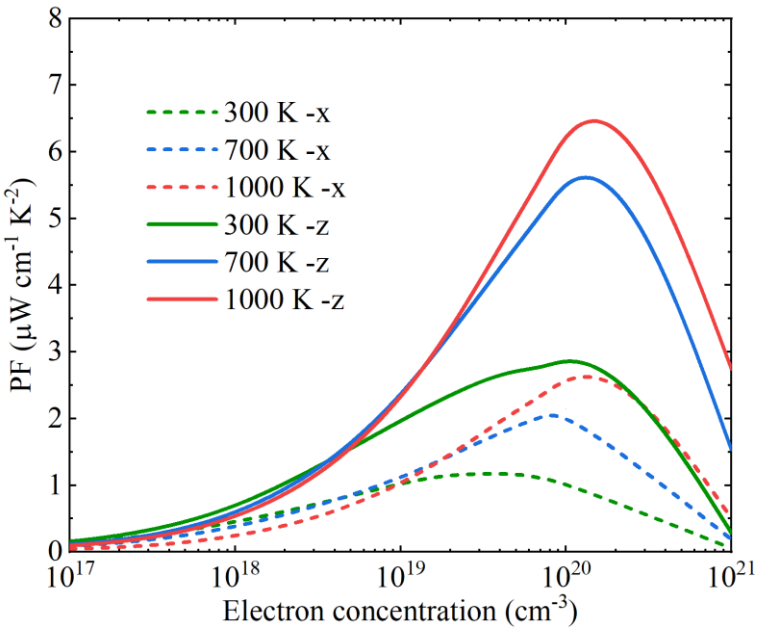

Figure. S6. The power factor (PF) for *n*-type $TlAgI_2$ along *x*- and *z*-direction at 300 K, 700 K, and 1000 K, respectively by HSE06 functional.

The thermal expansion coefficient (TEC) is defined as the rate at which a material expands with an increase in temperature. In more specific terms, this coefficient is determined at constant pressure and without a phase change, which implies that the material is expected to remain in its solid or fluid form. A range of strain values, spanning from 0.99 to 1.01, we selected under hydrostatic pressure conditions. The pressure was increased by 0.001 each time, resulting in the formation of 11 distinct

strained structures. The calculated thermal expansion for $TlAgI_2$ material is presented in Figure. S7.

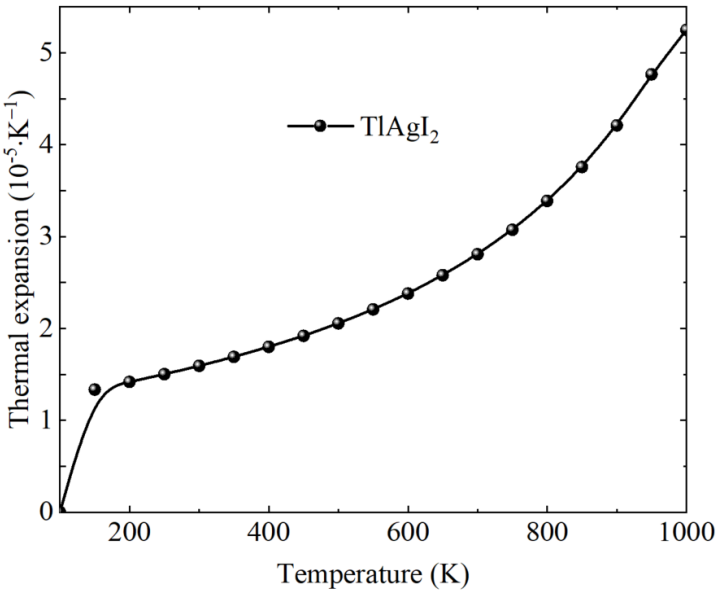

Figure. S7. The calculated thermal expansion coefficient (TEC) for $TlAgI_2$ in a wide temperature range.

The coefficient of thermal expansion for $TlAgI_2$ material is relatively modest. Nevertheless, we have calculated the impact of thermal expansion on lattice thermal conductivity and thermoelectric performance, as presented in Table SIII. It can be observed that the thermal conductivity of the $TlAgI_2$ material increases by 16.9 % [(0.069-0.059)/0.059] at 1000 K when the quasi-harmonic approximation (QHA) is considered. At 500 K, the ratio is 17.6% [(0.140-0.119)/0.119].

In order to investigate the influence of thermal expansion effects on thermoelectric performance, we have recalculated the *ZT* value based on harmonic approximation (HA) to be 3.54 at 1000 K. When considering QHA thermal expansion at 1000 K, the *ZT* values decreases from 3.54 to 3.35, resulting in a **5.36%** [(3.54-3.35)/3.54] reduction. At 500 K, the ratio is **4.21%** [(0.95-0.91)/0.95]. Given that the error is **5.36%** at 1000 K is acceptable and that the calculation is time-consuming, we have elected to provide the result without considering the thermal expansion. We hope to consider the lattice thermal expansion quantitatively in our future work.

Table SIII. The impact of thermal expansion on lattice thermal conductivity and thermoelectric performance.

	Thermal conductivity (HA+3ph)	*ZT* value
500 K	**0.119**	**0.95**
1000 K	**0.059**	**3.54**
500 K+QHA	**0.140**	**0.91**
1000 K+QHA	**0.069**	**3.35**

Furthermore, we cooperate the electronic transport performance by PBEsol functional into Supplemental Material for comparison as follows Figure. S8-S12.

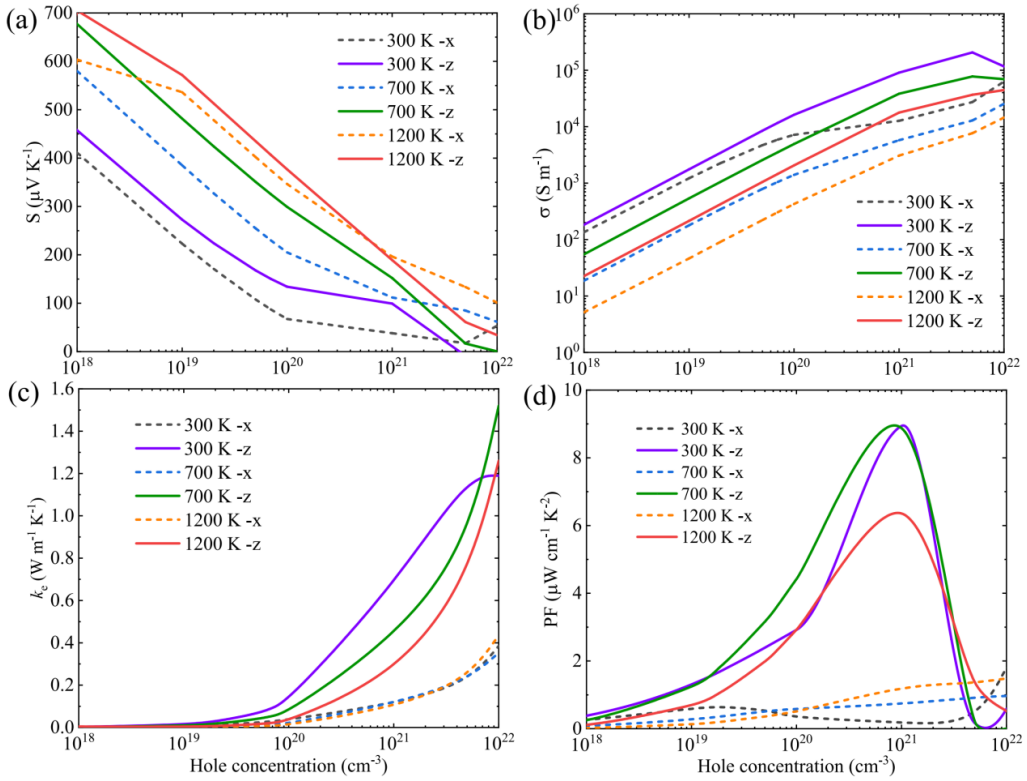

Figure. S8. The carrier transport performance of $TlAgI_2$. (a) The Seebeck coefficient, (b) Electrical conductivity, (c) Electronic thermal conductivity, (d) Power factor PF ($PF = S^2\sigma$) of the *p*-type with *x*-axis and *z*-axis, respectively by PBEsol functional.

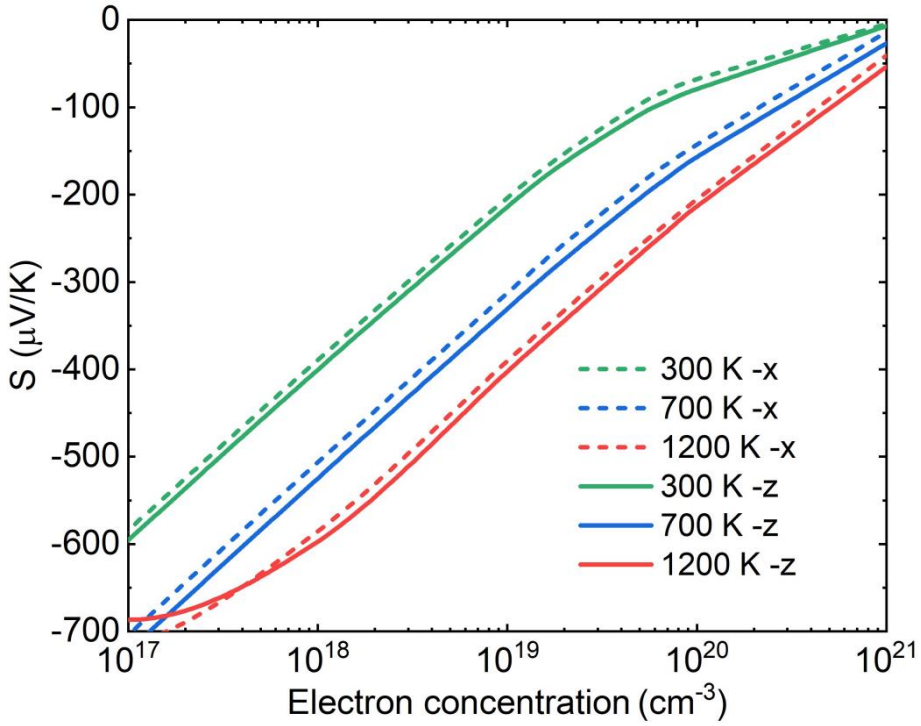

Figure. S9. The electronic transport performance of Seebeck coefficient for *n*-type $TlAgI_2$ along *x*- and *z*-direction at 300 K, 700 K, and 1200 K, respectively by PBEsol functional.

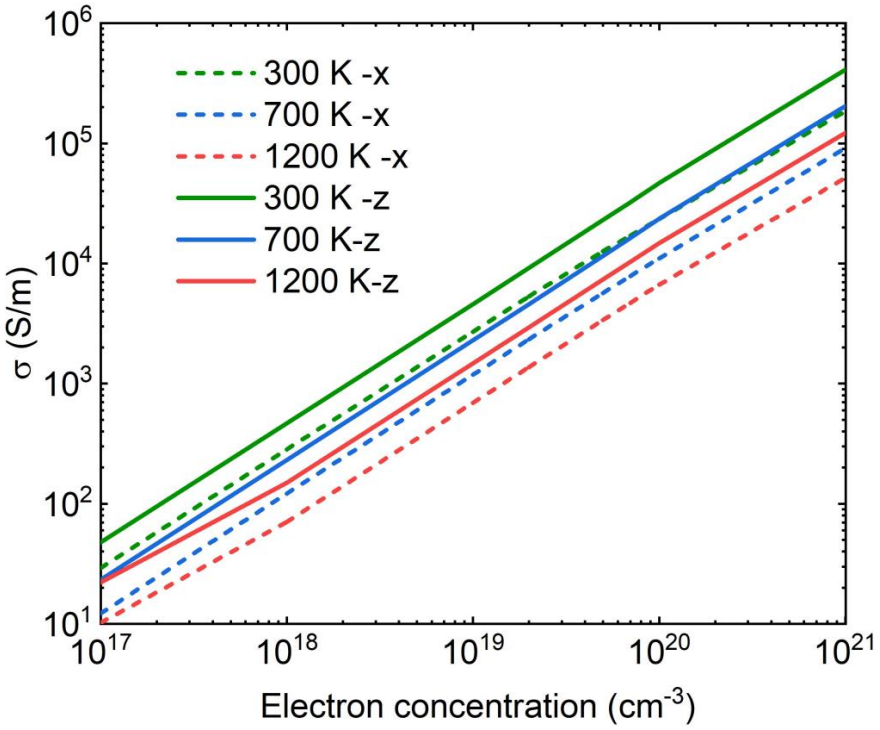

Figure. S10. The electronic transport performance of conductivity for *n*-type $TlAgI_2$ along *x*- and *z*-direction at 300 K, 700 K, and 1200 K, respectively by PBEsol functional.

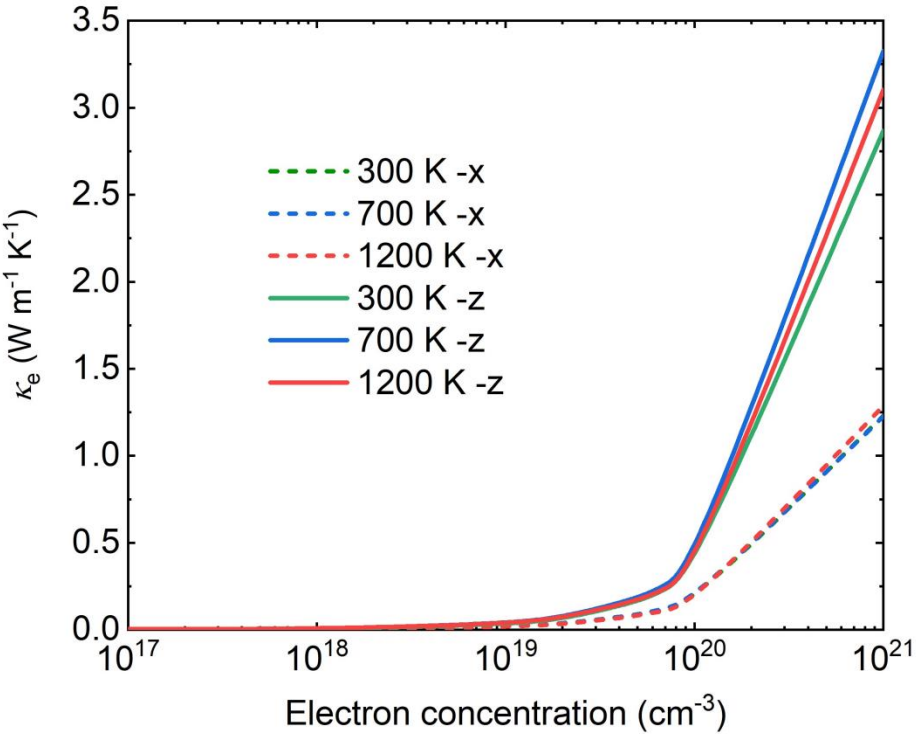

Figure. S11. The electronic transport performance of electronic thermal conductivity

along *x*- and *z*-direction for *n*-type $TlAgI_2$ at 300 K, 700 K, and 1200 K, respectively by PBEsol functional.

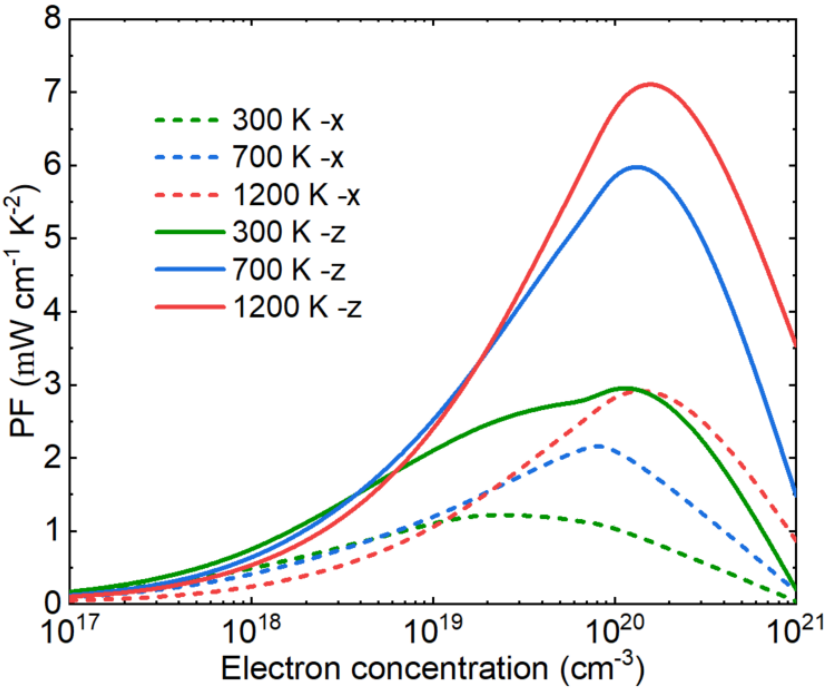

Figure. S12. The power factor (PF) for *n*-type $TlAgI_2$ along *x*- and *z*-direction at 300 K, 700 K, and 1200 K, respectively by PBEsol functional.

The crystal structure of $TlAgI_2$ (primitive cell) is as follows,

Tl2 Ag2 I4

1.0

-4.0942162416187280	4.0942162416187280	3.7809890008443361
4.0942162416187280	-4.0942162416187280	3.7809890008443361
4.0942162416187280	4.0942162416187280	-3.7809890008443361

Tl	Ag	I
2	2	4

Direct

0.2500000000000000	0.2500000000000000	0.0000000000000000
0.7500000000000000	0.7500000000000000	0.0000000000000000
0.2500000000000000	0.7500000000000000	0.5000000000000000
0.7500000000000000	0.2500000000000000	0.5000000000000000
0.8186663393760786	0.3186663393760787	0.1373326787521572
0.6813336606239214	0.8186663393760786	0.5000000000000000
0.1813336606239214	0.6813336606239214	0.8626673212478428
0.3186663393760786	0.1813336606239214	0.5000000000000000